We thank the reviewer for their constructive comments, which we believe have helped improve the quality of the manuscript. To address their concerns, we have made substantial revisions. Specifically, we have expanded and clarified the description of the coupling mechanism between the climate and ice sheet model. We have also added more discussions of our results in the context of previous studies of reconstructions. Detailed responses to the issues raised by them can be found below along with excerpts from the revised manuscript in boxes. A bibliography of the references cited here is present at the end of the document. We would like to emphasize that excerpts presented here are only a handful of the changes made to the manuscript, which are relevant to the reviewer's distinct comments. Besides these, there are many other changes designed to improve the overall appeal of the study.

Reviewer 1:
Specific comments:

1- Methods:
I found the coupling strategy not very clear. If I understand correctly, the surface mass balance model is a submodel of PSUISM. From Fig. 2 it seems that PSUISM only takes SAT, solar radiation, precipitation and Tocean. How these fields are downscaled onto the higher resolution ice sheet model grid? Then, what is the "solar radiation" (not explained in Sec. 2.3)? I find it a bit strange that surface albedo is not part of the fields that are given to PSUISM. Eq.1 and Eq.2 suggest that PSUISM compute its own albedo from rs and rl. Where do these rs and rl come from? Also, you do not explain how you compute the sub-shelf melt from Tocean. Is this a simple scaling after a bilinear spatial interpolation? What about ice shelves developing where there is no oceanic grid points (e.g. Kara and Barents seas)? I am sure that we can find all this information in the different papers that use a similar LOVECLIP framework but it would facilitate the reading to have a synthetic and integrated view in this paper as well.

A. We have now expanded the section on the climate-ice sheet coupling to be more complete and easier to read. First, we present answers to each specific question below:
   - LOVECLIM outputs of temperature, radiation and precipitation are downscaled using bilinear remapping and ocean temperature is downscaled using a conservative remapping approach.
   - Solar radiation refers to the incoming solar radiation at the surface (used in Eq. 3 for calculating the surface mass balance).
   - PSUIM calculates albedo based on the fraction of area that is covered by snow (r_s) and that without ($1 - r_s$) \. For the snow-covered areas, the fraction of area corresponding to wet and dry snow is also explicitly considered using the ratio between liquid water contained in the snow mass and the maximum embedded liquid capacity (r_l). All of this information is obtained from the last year of its previous chunk of PSUIM run. This provides a more realistic estimate of the albedo than downscaling from LOVECLIM.
   - The sub-ice-shelf ocean melting is calculated as per Pollard et al. (2015) using ocean temperature at 400m depth (T_o) from LOVECLIM as follows:
     $$OM = \frac{KK_T\rho_w c_w}{\rho_i L_f}\left|T_{oc} - T_f\right|\left(T_{oc} - T_f\right) \quad (5)$$
     where OM is the subshelf ocean melting rate (myr^{-1}), T_{oc} is the LOVECLIM ocean temperature at 400m depth (℃), T_f is the ocean freezing temperature at depth z (m) calculated as $T_f = 0.0939 - 0.057 \times 34.5 - 0.000764 \times z$, $K_T = 15.77myr^{-1}K^{-1}$ is a coefficient; K is a non-dimensional factor of order 1, $K = 3$; $\rho_w = 1028kgm^{-3}$ is the density of ocean water; $\rho_i = 910kgm^{-3}$ is the ice density; $c_w = 4218Jkg^{-1}K^{-1}$ is the specific heat of ocean water; and $L_f = 0.335 \times 10^6 Jkg^{-1}$ is the latent heat of fusion .
   - T_{oc}, used in calculating the ocean sub-ice-shelf melting (Eq. 5) is interpolated to PSUIM grid using conservative remapping. For some of the floating ice (shelves) in PSUIM (Eq. 2), the ocean points underneath may not get an ocean temperature assigned on interpolation from LOVECLIM, since the land-sea mask in LOVECLIM is kept constant. For each of such grid points, the algorithm averages over the neighboring eight PSUIM grid points and this process is repeated until all PSUIM ocean points get ocean temperatures.
     Eq. 2 referred here is:
     $$\left.\begin{array}{l} \rho_w(S - h_b) < \rho_i h;\ \text{and } h_s = h + h_b;\ \text{for grounded ice (ice sheet)} \\ \rho_w(S - h_b) > \rho_i h;\ \text{and } h_s = S + h\left(1 - \frac{\rho_i}{\rho_w}\right);\ \text{for floating ice (ice shelves)} \end{array}\right\} \quad (2)$$
     where $\rho_w = 1028kgm^{-3}$ is the density of ocean water; $\rho_i = 910kgm^{-3}$ is the ice density; S is the sea level (m); h_b is the bedrock elevation (m); h is the ice thickness (m); and h_s is the ice surface elevation (m).

We have now addressed all of these issues in the model description sections of PSUIM (Sect. 2.2) and LOVECLIP (Sect. 2.3). Some relevant sections from the revised manuscript are attached below.
The criterion for grounding and floating ice is defined in *Lines 151-154* in *Section 2.2*:

The ice is determined to be grounded or floating based on buoyancy, as per:

$$\left.\begin{array}{l} \rho_w(S-h_b) < \rho_i h;\ \text{and}\ h_s = h + h_b;\ \text{for grounded ice (ice sheet)} \\ \rho_w(S-h_b) > \rho_i h;\ \text{and}\ h_s = S + h\left(1-\frac{\rho_i}{\rho_w}\right);\ \text{for floating ice (ice shelves)} \end{array}\right\} \quad (1)$$

where $\rho_w = 1028 kgm^{-3}$ is the density of ocean water; $\rho_i = 910 kgm^{-3}$ is the ice density; S is the sea level (m); h_b is the bedrock elevation (m); h is the ice thickness (m); and h_s is the ice surface elevation (m).

Calculation of the ocean sub-ice-shelf melting is defined in *Lines 175-181* in *Section 2.2*:

The sub-ice-shelf ocean melting is calculated as per Pollard et al. (2015) using ocean temperature at 400m depth (T_o) from LOVECLIM as follows:

$$OM = \frac{KK_T\rho_w c_w}{\rho_i L_f}\left|T_{oc} - T_f\right|\left(T_{oc} - T_f\right) \quad (5)$$

where OM is the subshelf ocean melting rate (myr^{-1}), T_{oc} is the LOVECLIM ocean temperature at 400m depth (°C), T_f is the ocean freezing temperature at depth z (m) calculated as $T_f = 0.0939 - 0.057 \times 34.5 - 0.000764 \times z$, $K_T = 15.77 myr^{-1}K^{-1}$ is a coefficient; K is a non-dimensional factor of order 1, $K = 3$; $c_w = 4218 Jkg^{-1}K^{-1}$ is the specific heat of ocean water; and $L_f = 0.335 \times 10^6 Jkg^{-1}$ is the latent heat of fusion.

Downscaling of solar radiation, albedo and subshelf melting over locations without oceanic grid points in LOVECLIM are explained further in *Lines 250-257* in *Section 2.3*:

Surface incoming shortwave radiation from LOVECLIM (Q, Eq. (3)) is bilinearly interpolated to PSUIM grid and then used to calculate the surface mass balance. PSUIM calculates albedo using snow covered fraction (r_s) and the ratio between liquid water contained in the snow mass and the maximum embedded liquid capacity (r_l) from the last year of its previous chunk. This provides a more realistic estimate of the albedo than downscaling from LOVECLIM. T_{oc}, used in calculating the ocean sub-ice-shelf melting (Eq. 5) is interpolated to PSUIM grid using conservative remapping. For some of the floating ice (shelves) in PSUIM (Eq. 2), the ocean points underneath may not get an ocean temperature assigned on interpolation from LOVECLIM, since the land-sea mask in LOVECLIM is kept constant. For each of such grid points, the algorithm averages over the neighboring eight PSUIM grid points and this process is repeated until all PSUIM ocean points get ocean temperatures.

On the coupling strategy again, but from the ice sheet to the climate model this time. I understand the use of the acceleration factor. However, I do not understand how you can ensure water conservation between the ice sheet and the rest of the climate system with this acceleration factor. It seems to me that when we use an acceleration factor we can only conserve the volume or the flux, but not the two quantities at the same time (already reported by Heinemann et al., 2014). For example, let's assume that the ice sheet model runs 10 years for each year computed by the rest of the climate model. Let's say that the ice sheet model produces 10 km3 of volume loss integrated over the 10 years (1km3/yr). What do you give to the ocean model? 1 km3 or 10 km3 ? The second option conserves the volume but the fluxes that arrive to the ocean are overestimated which can ultimately result in unrealistic oceanic evolution. In any case, I think it needs a bit more of description in the paper. Also, what is the routing strategy to transfer the ice loss to the ocean? Do you use the atmospheric model runoff model? In case of an ice sheet inception, do you have a negative flux at the surface of the ocean that increases the salinity? Is this spatially resolved?

A. In the current setup, we are conserving freshwater flux and not the freshwater volume. As the reviewer rightly points out, conserving the net volume instead would lead to huge fluxes into the ocean. However, as we are conserving flux, there is an underestimation of the net freshwater volume and thus could lead to unrealistic circulation changes. This meltwater flux from the ice model is dynamically routed based on PSUIM topography till it reaches the ocean or the domain edge, and then is routed to the nearest ocean grid point in LOVECLIM. During an inception, since the precipitation is used for building ice, the runoff from PSUIM into LOVECLIM is reduced, which in turn increases the salinity in the ocean. This salinity change is spatially resolved.

We have now added discussions regarding this in *Lines 263-273* in *Section 2.3*:

> The total meltwater from basal melting and liquid runoff in PSUIM is dynamically routed based on PSUIM topography till it reaches the ocean or the domain edge, and then is routed to the nearest ocean grid point in LOVECLIM. The calving flux is channeled into CLIO's iceberg model (Schloesser et al., 2019;Jongma et al., 2009) in the Southern Hemisphere (SH) and as an iceberg melt flux (freshwater flux and heat flux) in the NH (Schloesser et al., 2019). While both freshwater flux and freshwater volume cannot be simultaneously conserved in an accelerated run (Heinemann et al., 2014), we conserve freshwater flux in the current setup. The primary rational for this being that surface freshwater and meltwater fluxes are balanced by the convergence of ocean salt fluxes in equilibrium states, and adjustments of the ocean circulation are thought to occur rapidly compared to those of ice sheets. PSUIM is forced by LOVECLIM precipitation and LOVECLIM by PSUIM runoff. During a glacial inception (termination), the runoff from PSUIM into LOVECLIM reduces (increases) as ice sheets grow. This reduction (increase) in runoff into the ocean, relative to the evaporation, increases (decreases) the salinity of the ocean. This salinity change is spatially resolved.

Have you run a pre-industrial control run (for example a 10-kyr long simulation with the LGM bathymetry under pre-industrial orbital and GHG forcing)? Such simulation could be nice to validate your model setup, or at least to quantify the bias in the coupled model trajectory.

A. We ran a pre-industrial control run with constant forcings set at 1850 with LGM bathymetry. The figure is attached below for reference.

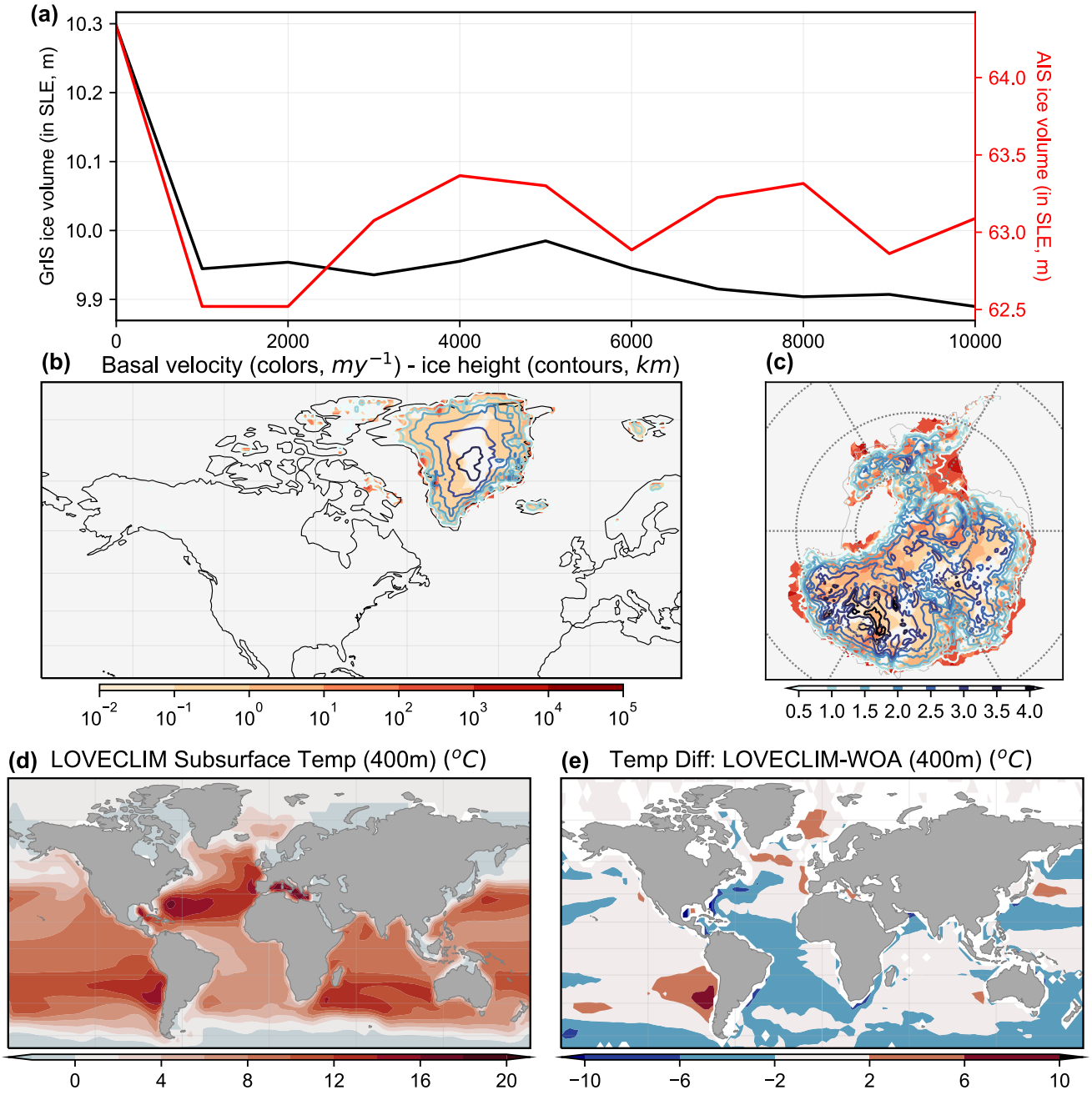

Figure R1: LOVECLIP simulation forced with constant 1850 forcing and LGM bathymetry. (a) Simulated ice volumes over Greenland (black) and Antarctica (red) in sea level equivalents (m). (b) Equilibrium basal ice velocity (solid colors, my^{-1}) and ice thickness (colored contours, km) for NH. (c) Same as (b) but for SH. (d) Equilibrium subsurface ocean temperature at 400m depth simulated by LOVECLIM. (e) Subsurface ocean temperature difference between LOVECLIM and WOA (Locarnini et al., 2013) dataset.

We have clarified in the text now that the biases are based on present day simulations using an LGM bathymetry and that we do not find large-scale differences in the biases when running with present day bathymetry. This is addressed in *Lines 228-230* in *Section 2.3*:

> These LOVECLIM biases are calculated for PD simulations using an LGM bathymetry. We did compare the biases between using a PD or LGM bathymetry, and while there were regional differences, the large-scale structure was found to be similar (not shown).

By starting at 240 ka, you start towards the end of a deglaciation. Do you think that the long-term climate trajectory has an impact on your results? For example do you think that a restart from a full glacial state at 250 ka would result in a similar global ice volume evolution across MIS7?

A. We agree with the reviewer's comment that our simulated evolution could depend on the initial condition. To restart the model from 250ka with realistic ice volumes, we would need initial conditions at that time that comes from re-running the whole setup from the previous interglacial, MIS 9 (~320ka). If we get a realistic inception and the re-adjusted parameter set can simulate a termination into MIS 7e, then we expect to get a similar ice volume evolution across MIS 7. We fully acknowledge that our results are dependent on the parameter choices and are sensitive to the initial conditions. We have now addressed this in *Lines 543-545* in *Section 4*:

> The simulated ice sheet volume is well within the range of reconstructions for a rather narrow range of parameters. Small changes in parameter values can produce strongly diverging trajectories, and the emergence of multiple equilibrium states may also suggest the model's dependence on initial conditions.

You use a simple bias correction for surface temperature and precipitation. Why not use a similar technique for the radiative inputs of the ice sheet model and for the oceanic temperature as well?

A. Thank you for this suggestion. We agree that including additional bias corrections as suggested above might further improve the representation of ice sheets in our model, however, neither radiation nor ocean temperature bias correction is implemented in the model version used for this study. We have recently started experimenting with implementing ocean temperature bias correction, and found that this helps simulating a somewhat more realistic, present-day Antarctic ice sheet. The effects on Northern Hemisphere ice sheets appear to be relatively smaller, presumably because of smaller coastal ocean temperature biases (e.g., Fig. R1). We have included this in the discussion for future improvements in *Lines 561-569* in *Section 4*:

> Nevertheless, there is scope of further improving the current setup. For instance, we only implement temperature and precipitation bias corrections in the current setup, and including bias corrections for radiation and ocean temperature might improve our representation of ice sheets. Future research might further improve the current setup by including the advective precipitation downscaling scheme (Bahadory and Tarasov, 2018) to account for orographic forcing, which is not captured in LOVECLIM. We are also investigating the possibilities of using a dynamical, an altitude-dependent and a CO_2-dependent lapse rate corrections while downscaling temperature from LOVECLIM to PSUIM. This is because the atmospheric lapse rate depends on the atmospheric CO_2 concentration – an effect that has not been considered so far in glacial dynamics. Furthermore, improving our basal sliding coefficient map for the NH using information of sediment sizes, instead of simply using a binary coefficient map, has the potential of further improving the simulations.

The hydrofracturing and cliff collapse parametrisation embedded in PSUISM is controversial (e.g. Edwards et al., 2019). Do you think that you would end up with different ice volume trajectories using a model that does not account for the MICI?

A. The contributions from hydrofracturing and cliff instabilities were negligible in our simulations and hence were not presented in the mass balance figure. Just to be sure, we repeated our analysis with hydrofracturing and cliff melt inactive in PSUIM and found no change in our ice evolutions. This is mentioned in *Lines 320-322* in *Section 3.1*:

> Following the concerns raised in Edwards et al. (2019), we ran a BLS simulation with hydrofracturing and cliff instability inactive and found no differences in the ice evolutions. This finding illustrates the complexity of the task to better constrain associated parameters in comparison of paleo climate simulations and data.

We also added discussions on the implication of these parameterizations for future studies in *Lines 546-551* in *Section 4*:

> In this context, we note that parameterizations associated with hydrofracturing and cliff instability did not impact our ice sheet trajectories. These processes have provided substantial contributions to the rapid Antarctic ice sheet retreat simulated in response to future climate projections (DeConto and Pollard, 2016), and better constraining these parameterizations is important to reduce uncertainties related to future sea level trajectories (e.g., Edwards et al., 2019). Presumably, these processes did not play an important role in our present simulations, because the climate is generally too cold, suggesting that opportunities for constraining these parameters in glacial simulations may be limited.

2- Results:

From my understanding of your model results, the respective role of orbital configuration with respect to CO2 is pretty much linked to the choice of the alpha / m combination. From Fig. 3 it seems that you cannot guarantee the uniqueness of your calibrated alpha / m (higher m but lower alpha might works equally well than lower m and higher alpha). As a result how robust is your conclusion on the respective role of orbital versus CO2?

A. Although we agree that results presented here could be influenced by parameter values, we believe our results to be robust over this time period. While Figure 3 showed only a handful of ensembles that best explain the effects of the *'α'* and *'m'* parameters, the Fig. S3 (underneath) shows the whole ensemble of simulations considered in the study. These ensembles correspond to different values of *'α'*, *'m'*, acceleration factor, $N_A = T_P/T_L$ (PSUIM chunk length corresponding to LOVECLIM chunk length), and the maps of sliding coefficient *'C'*, in Eq. (6) and Eq. (7):

$$\widetilde{u_b} = C'|\tau_b|^{\mu-1}\widetilde{\tau_b}\ , \qquad (6)$$

where $\widetilde{u_b}$ is the basal sliding velocity, $\widetilde{\tau_b}$ is the basal stress; μ is the basal sliding exponent (=2); C' is the basal sliding coefficient which is a function of the basal homologous temperature:

$$C' = (1-r)C_{froz} + rC(x,y)\ , \qquad (7)$$

with $r = max\left[0, min[1,(T_b+3)/3]\right]$; where T_b(°C) is the basal homologous temperature relative to the pressure melting point ($T_m = -0.000866h$, h being the ice thickness in m); and $C_{froz} = 10^{-20}$m yr^{-1}Pa^{-2} (which cannot be zero to avoid numerical inconsistencies but is small enough to allow essentially no sliding).

We tried different combinations of all the parameter sets and have updated Table 1 to show all the ensemble runs performed in this study. While we performed a total of 50 separate experiments, we reported only 15 of them in Figure 3 that best describe the parameter sensitivities. We have now clarified this in in *Lines 293-300* in *Section 2.4:*

> Furthermore, sensitivity experiments with different GHG sensitivities (α, Sect. 2.1) and melt parameterizations (m, Sect. 2.2) are run with full forcing. Generally, higher α leads to a stronger sensitivity to CO_2 concentrations, and higher values of m strengthen buildup and weaken melting of ice during interglacial climates. These experiments are presented in the first row of Table 1 (1-15) and Fig. 3. Additional simulations with different combinations of acceleration (N_A), GHG sensitivity (α), melt parameter (m), basal sliding coefficient maps over the NH ($C(x,y)$) and higher ice model resolution (0.5 × 0.25° for NH, 20 × 20 km polar stereographic for Antarctica*)* have been performed (experiments 16-50 in Table 1). The whole ensemble of simulations is presented in Fig. S3. Although we note that these experiments do not present a systematic evaluation of the full parameter space, ice sheet trajectories are consistent with and thereby support the conclusions presented in this paper.

The updated *Table 1* is as below:

Expt Number	Orb Forced	GHG Forced	N_A	α	m (Wm^{-2})	C (myr^{-1}Pa^{-2})-NH
1 **(BLS)**	**Y**	**Y**	**5**	**2**	**125**	
2	**N**	**N**	5	2	125	
3	Y	**N**	5	2	125	
4	**N**	Y	5	2	125	Binary distribution
5	Y	Y	5	2	125	
6	Y	Y	5	**1.8**	125	**1.**Ocean: $C(x,y)$=10^{-6}; representing deformable sediments
7	Y	Y	5	**2.2**	125	
8	Y	Y	5	**2.5**	125	
9	Y	Y	5	**3**	125	
10	Y	Y	5	2	**80**	**2.**Land: $C(x,y)$=10^{-10}; representing non-deformable rock.
11	Y	Y	5	2	**100**	
12	Y	Y	5	2	**120**	
13	Y	Y	5	2	**130**	
14	Y	Y	5	2	**140**	
15	Y	Y	5	2	**150**	
16-20	*Y*	*Y*	*5*	***1.5***	***120,125,130,140,150***	
21-24	*Y*	*Y*	*5*	***3.5***	***80,100,120,125***	
25-27	*Y*	*Y*	***1 (30ky run)***	*2*	***110,120,130***	*Binary*
28-30	*Y*	*Y*	***2 (30ky run)***	*2*	***110,120,130***	
31-33	*Y*	*Y*	***10***	*2*	***110,130,150***	

34-36 *37-38*	*Y* *Y*	*Y* *Y*	***10*** ***20***	***2.5*** ***2.5, 3***	***110,120,130*** *125*	
39-41 *42-44* *45-47*	*Y* *Y* *Y*	*Y* *Y* *Y*	*5* *5* *5*	*2* *2* ***2.5***	*125* ***150*** *125*	*Tertiary* ***1.***<u>*Ocean:*</u> $C(x,y)=10^{-6}$; ***2.1*** <u>*Land (soft tills):*</u> $C(x,y)=\mathbf{10^{-7},10^{-8},10^{-9}}$ *over northeastern North America* ***2.2*** <u>*Land (hard bed):*</u> $C(x,y)=10^{-10}$
High Resolution Runs: 0.5 × 0.25° *for NH*, 20 × 20 km *polar stereographic for Antarctica*						
48-50	*Y*	*Y*	*5*	*2*	***110,130,150***	*Binary*

Table 1: List of all ensemble runs performed for the study study (shown in Fig. S3). The first 15 experiments are discussed in Sect. 3.1 and shown in Fig. 3. Values in bold represent the difference from the baseline simulation (BLS, experiment number 1). N_A represents the PSUIM vs LOVECLIM acceleration factor (Sect 2.3). α represents the GHG sensitivity scaling factor (Eq. 1, Sect. 2.1) and m represents the constant parameter in the surface energy balance equation (Eq. 3, Sect. 2.2). C represents the basal sliding coefficient map used for the NH (Eq. 7, Sect. 2.2). All experiments are run at 1 × 0.5° resolution for the Northern Hemisphere and 40 × 40 km polar stereographic resolution for Antarctica. The experiments in italics (16-50) are not presented here but were also performed to better constrain the parameter sensitivities.

The whole ensemble of experiments is shown under in Fig. S3 (in supplementary):

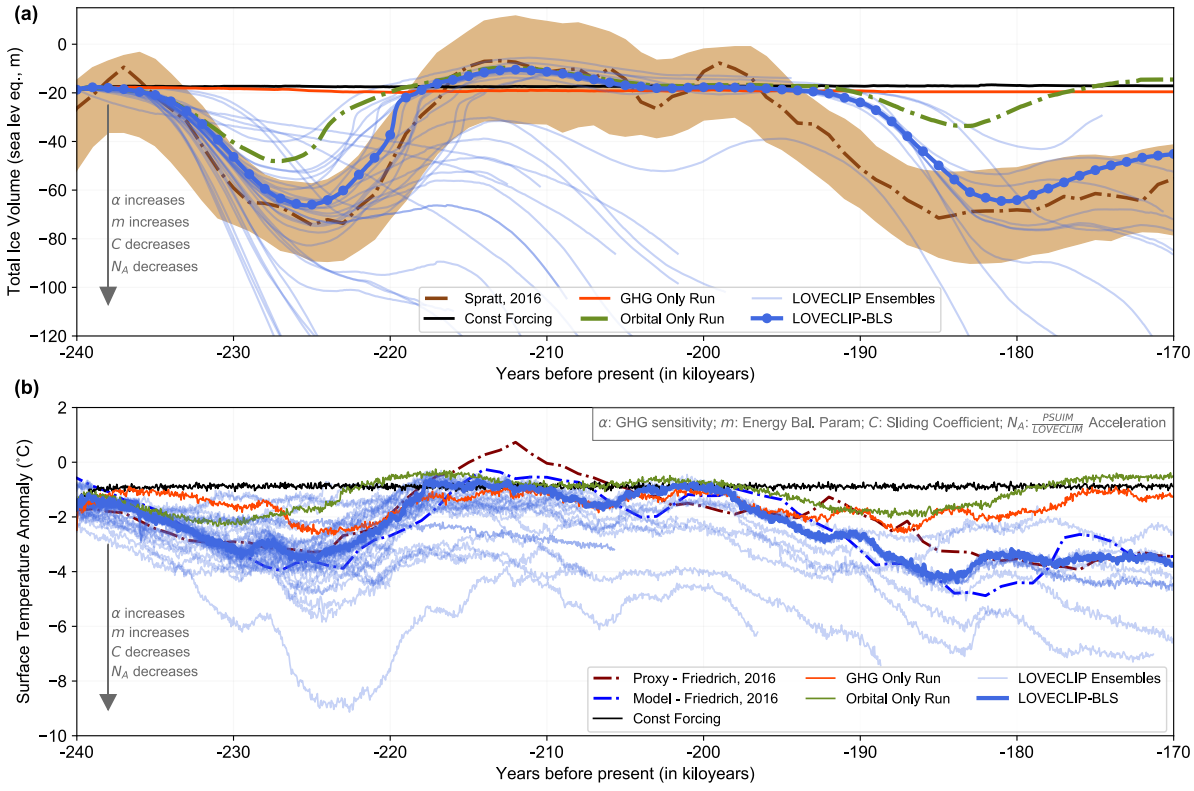

Figure S3: Transient LOVECLIP ensemble simulations over MIS7 with varying GHG sensitivities (α = 1.5-3.5), energy balance parameter (m = 80-150Wm^{-2}), basal sliding coefficient (C = 10^{-6}-10^{-8} myr^{-1}Pa^{-2}) and PSUIM-vs-LOVECLIM acceleration factor (N_A = 1,2,5,10,20). The best results are obtained for α=2, m=125 Wm^{-2}, binary sliding map (ocean: C=10^{-6} myr^{-1}Pa^{-2} and land: C=10^{-8} myr^{-1}Pa^{-2}) and N_A=5 (experiment 1 in Table 1, BLS).

Although we could get the model to glaciate from MIS 7e to MIS 7d for a low *'α'* and high 'm', the model does not terminate from the glaciation of MIS 7d.

Further, to verify our result that glacial inceptions are driven primarily by orbital forcings, we performed orbital-only simulations with CO_2 values of 180,200,220,240,260 and 280 ppmv in Fig. R2. These runs are similar to the blue line in Figure 5 (and the green line in Fig. S3 above), but with different background CO_2 values instead of keeping CO_2 constant at 240ka values (~245 ppmv). The results suggest that we can get a glacial inception over MIS 7e-7d, even for a high CO_2 value of 280 ppmv. Thus, we think our conclusion of glacial inceptions being primarily driven by orbital forcings is robust over this period.

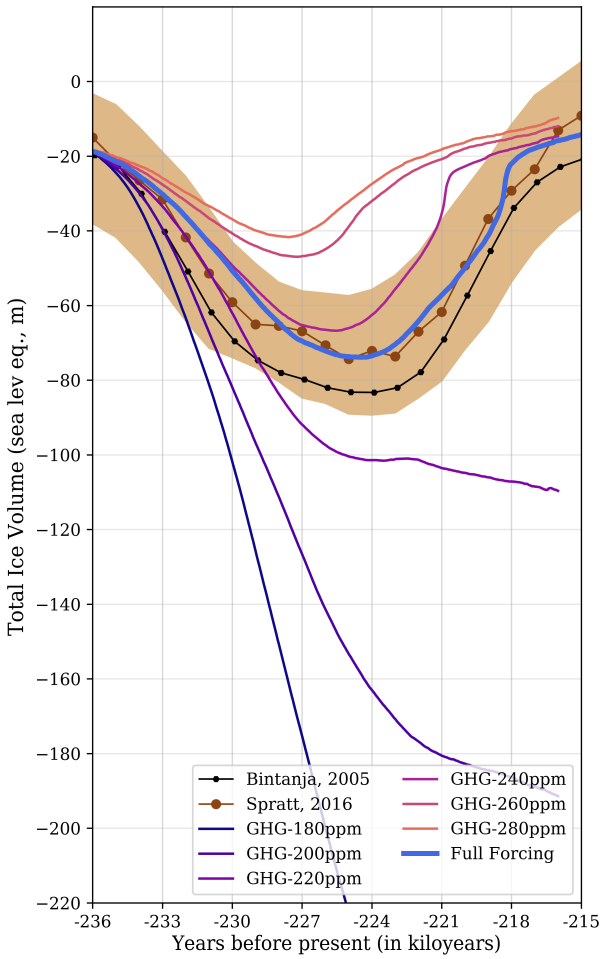

Figure R2: LOVECLIP simulations forced with transient orbital forcings, but constant background CO_2 values. All experiments are conducted with an α value of 2 and m of 125 Wm^{-2}.

You justify the use of the alpha parameter to correct for the lack of sensitivity of the climate model. There are alternative way to modify the climate sensitivity in the model. For example Loutre et al. (2011) modify a set of model parameters in order to have a similar pre-industrial climate but different sensitivity to the change in CO2. With your approach you might give too much importance to the radiative effect of CO2.

A. We agree that climate sensitivity could depend on responses to many different forcings. Here, we use a simple alpha parameter to change only the longwave sensitivity to CO_2, and not to other greenhouse gases. We have acknowledged this in *Lines 122-134* in *Section 2.1*:

The effect of CO_2 variations with respect to the reference CO_2 concentration (356 ppm) on the longwave radiation flux is scaled up by a factor α (Eq. 1), to account for the low default sensitivity of ECBilt to changes in CO_2 concentrations (Friedrich and Timmermann, 2020;Timmermann and Friedrich, 2016;Timm et al., 2010). The effect of CO_2 on the longwave radiation is given as:

$$LWR = \alpha . a(\lambda, \phi, p, t_{season}) . \log\left[\frac{CO_2(t)}{CO_2^{ref}}\right] \quad (1)$$

where LWR is the longwave radiation flux from CO_2; α is our scaling factor for the transfer coefficient, a, which is a function of longitude, latitude, height and season; CO_2^{ref} is the reference CO_2 value set at 356 ppm. α changes the sensitivity of our model. For reference, the equilibrium climate sensitivity for CO_2 doubling is 3.69K for α of 2. Climate sensitivity is a non-trivial measure that can be changed in many different ways. For instance, changing the cloud parameterization or surface parameters would change both the longwave and shortwave forcings. Adjusting multiple

parameters may not necessarily lead to more realistic simulations. While it is possible that the climate sensitivity to some of the other forcings are also weak (Timm and Timmermann, 2007), we use a simple alpha (α) parameter to change only the longwave sensitivity to CO_2, and not to other greenhouse gases. α is determined based on transient past and future simulations.

The Eurasian ice sheet in your simulation does not grow at all which seems in contra- diction with palaeo data (e.g. Batchelor et al., 2019). Even in the run-away glaciation presented in Fig. S6, it seems that there is only very little ice developing in Eurasia. I know that it is not trivial to simulate satisfactorily the Eurasian ice sheet inception, particularly the Kara-Barents sector. Do you have any idea on how to improve on this? Do you think that it is an oceanic problem, e.g. too warm waters in the Kara and Barents seas? Or an atmospheric problem, e.g. shift in storm tracks?

A. We think this to be primarily an atmospheric problem because of the coarse T21 resolution and 3-layered atmosphere of LOVECLIM; and the best way to improve on this would be to use a model with more realistic atmosphere. We have now added more discussions on our ice sheet distribution in *Lines 344-376* in *Section 3.2*:

In the context of previous modelling studies and geological records over this MIS 7-6 period, our ice sheet distribution at MIS 7c (212ka, Fig. 4g and 219.5ka, Fig. S7) is very similar to that reported in Colleoni and Liakka (2020). However, we simulate a stronger inception compared to that of Colleoni et al. (2014b) over the corresponding 236-230ka period. They also reported a bifurcated but connected North American ice sheet at MIS 6 (157ka) from both their control (100km) and high resolution (40km) experiments. Our simulation results in separate Laurentide and Cordilleran ice sheets but generates neither a Eurasian nor a Siberian ice sheet, albeit at 170ka. On a side note, our North American ice sheet distribution at 180ka (Fig. 7) is closer to that of Colleoni and Liakka (2020) at 157ka. Studies of NH reconstructions during MIS 6 such as Svendsen et al. (2004), over 160-140ka, Rohling et al. (2017), around 140ka, and Batchelor et al. (2019), over 190-132ka, have all reported glacial geological records to indicate a larger extent of the Eurasian ice sheet at MIS 6 glacial maximum compared to the LGM, while our simulations only show a persistent Fenno-Scandian ice sheet and a relatively small Eurasian ice sheet at 170ka. More recently, Zhang et al. (2020) reported the existence of a Northeast Siberia-Beringian ice sheet at MIS 6e (190-180ka) using NorESM-PISM simulations validated by North Pacific geological records. However, our model does not simulate any ice over Alaska, Beringia and northeast Siberia over MIS 7-6.

Our model's difficulty in simulating the Eurasian ice sheet can be attributed to the competition between Laurentide and Eurasian ice sheet growth, which makes it arduous to realistically simulate them simultaneously alongside generating the right atmospheric patterns. Some previous studies have suggested that teleconnections from stationary wave patterns induced by a large Laurentide ice sheet could lead to warming over Europe and influence Eurasian ice sheet evolution (Roe and Lindzen, 2001;Ullman et al., 2014). The Laurentide building up first in our simulations could have changed the storm tracks and dried out Eurasia. It is also worth reiterating that LOVECLIM has a coarse T21 grid with a simple 3-layered atmosphere. While the circulation changes reported here maybe model dependent, Lofverstrom and Liakka (2018) reported that at least a T42 grid was needed in their atmospheric model (CAM3) to generate a Eurasian ice sheet using SICOPOLIS, albeit for the LGM. They attribute this discrepancy to lapse rate induced warming due to reduced and smoother topography and higher cloudiness leading to increased re-emitted longwave radiation towards the surface. These teleconnection patterns are further discussed in Sect. 3.6. Our LOVECLIM setup also uses a fixed lapse rate for downscaling LOVECLIM surface temperatures (Eq. 10 and 11), while both Roche et al. (2014) and Bahadory and Tarasov (2018) used a dynamic lapse rate, which is estimated locally for the ice model grids in each LOVECLIM grid. Bahadory and Tarasov (2018) reported ice thickness differences up to 1km on using the dynamic lapse rate scheme compared to a fixed 6.5˚Ckm^{-1}. Nevertheless, for runaway trajectories, our model can build up a Eurasian ice sheet for ice volumes greater than -200m SLE once the Laurentide growth slows down (not shown). Our modelling setup also does not account for sub-grid mass balances, which can be especially relevant over mountainous regions with large sub-grid relief such as Alaska (Le Morzadec et al., 2015). Coarse grids tend to average out tall peaks and low valleys and thus don't capture the non-linear combination of accumulation zones on the high peaks and ablation zones in the valleys. These shortcomings could explain the lack of Eurasian, Siberian and Beringian ice sheets in our simulations.

And acknowledged this in the discussion in *Lines 556-558* in *Section 4*:

Our present setup has difficulties in realistically simulating both Laurentide and Eurasian ice sheets simultaneously and generates a smaller Eurasian ice sheet compared to reconstructions, which could be a model dependent feature of

LOVECLIM, given it is a T21 grid with only three levels in the atmosphere, and so could vary with the choice of the climate model used.

While the runaway simulation in Fig. S6 (Fig. S9 in the revised version) shows a very small Eurasian ice sheet, our Eurasian ice sheet grows once Laurentide growth slows down for ice volumes > 200m SLE (Fig. R3). This suggests that the relatively small Eurasian may not result from large biases in the Barents-Kara sector (also see subsurface temperature biases in Fig. R1 above), but from the timing of Laurentide and Eurasian growth alongside changes in atmospheric patterns.

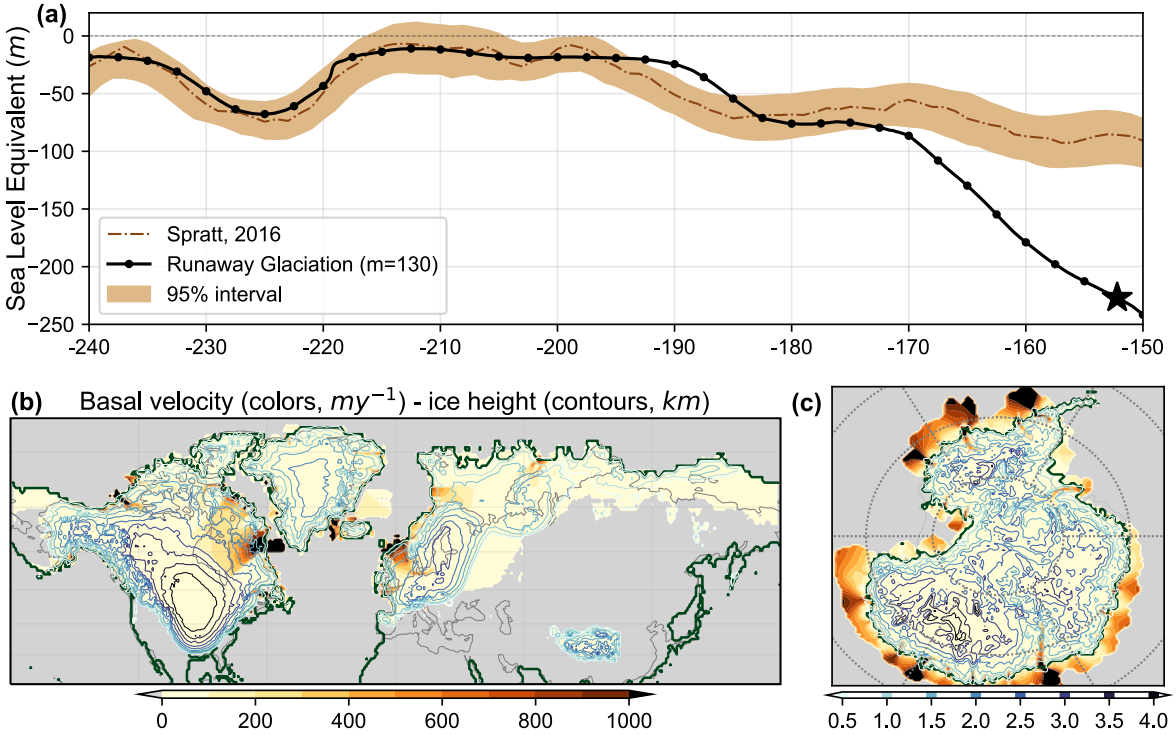

Figure R3: Transient LOVECLIP simulation with α=2 and m=130 Wm^{-2} (runaway simulation). (a) Sea level reconstruction (m) and 95% confidence interval of Spratt and Lisiecki (2016) (brown). Total ice volume from LOVECLIP run in black (SLE, m). The star shows ice volume at 152ka corresponding to 225m. (b) Basal ice velocity (solid colors, my^{-1}); ice thickness (colored contours, km) and the grounding line (solid green lines) for the Northern Hemisphere at 152ka. (c) Same as (b) but for Southern Hemisphere.

For the two step inception (Sec. 3.4), you claim that CO2 explains the later full inception. If the insolation signal is indeed similar for both periods, it shows nonetheless a greater amplitude in MIS 7e-7d-7c with respect to MIS 7a-6e-6d. The insolation maxima is thus slightly smaller for the later period. This slight difference in the insolation maxima could explain the ice retreat in the older inception, with the full glaciation being the result of an insolation threshold? Of course CO2 should help but it is hard to distinguish the role of the two forcings (especially also because the results depend on the value of the chosen alpha parameter).

A. We agree with the reviewer that the insolation maximum is indeed smaller for the later period (Figure 6a). But we believe CO_2 to drive the later inception because our orbital only run shows a much weaker inception and subsequent termination over MIS 7a-6e-6d compared to MIS 7e-7d-7c in Figure 5. We have now clarified this in *Lines 408-415* in *Section 3.4*:

In spite of orbital forcing being similar over the second half of the composite figure, model trajectories diverge markedly. The successful glacial termination coincides with increasing CO_2 concentrations (dashed line), whereas the aborted termination during MIS 6e-6d (180-170ka, solid line) is associated with flat-lined glacial CO_2 values (Fig. 6a-6c). Although the insolation maximum is weaker for the later period (MIS 7a-6e-6d) compared to the earlier period (MIS 7e-7d-7c), we argue the full inception of the later period to be primarily driven by changes in CO_2. This is further supported by the orbital-only run showing a substantially weaker inception and subsequent termination over MIS 7a-6e-6d compared to MIS 7e-7d-7c (Figure 5), suggesting that the latter full inception could not be attributed only to an insolation threshold.

I wonder how robust are the atmospheric circulation changes discussed in Sec. 3.6. For example, don't you think that the atmospheric circulation might be potentially largely affected by the presence of an ice sheet in Eurasia?

A. A high pressure cold anticyclonic pattern over ice sheets such as the Laurentide has previously been reported and was shown to be robust by Roe and Lindzen (2001). They suggest a balance between precipitation maxima alongside increased melting over the south western edges from warmer winds upslope and reduced precipitation over the rest of the ice sheet due to cold northerly winds can lead to either an equilibrium ice sheet configuration or runaways in either directions. However, it goes without saying that such patterns and runaways could change when using more realistic atmospheric models. While the presence of a Eurasian ice sheet would definitely affect the atmospheric circulation, we believe the Laurentide developing rapidly in our simulation changes the atmospheric circulation causing some warming over Europe and changed storm tracks that prevent the growth of a Eurasian ice sheet. As mentioned in the response to a previous question, our model simulates a Eurasian ice sheet only when the Laurentide growth slows down. While the circulation changes reported here maybe model dependent, Lofverstrom and Liakka (2018) reported that at least a T42 grid was needed in their atmospheric model (CAM3) to generate a Eurasian ice sheet using SICOPOLIS, albeit for the LGM. We have now mentioned this in *Lines 488-493* in *Section 3.6*:

> Roe and Lindzen (2001) suggested that the topography of an ice sheet such as the Laurentide induces a high-pressure anticyclonic circulation over the western end of the ice sheet. The associated cooling and upslope flow lead to enhanced rainfall over the western and southwestern ends of Laurentide. However, the prevailing cold northerlies downslope cause a reduction in rainfall over the ice sheet. This interplay between cooling associated with anticyclonic circulations alongside enhanced rainfall over western Laurentide and the reduction in rainfall over most of the ice sheet due to cold northerlies, can lead to an equilibrium ice sheet configuration or ice sheet growth/decay.

and in *Lines 516-522* in *Section 3.6*:

> While these stationary wave feedbacks are similar to the ones described by Roe and Lindzen (2001) and they suggested these patterns to be robust for a range of parameters, it is possible that such circulation patterns could change when using a more realistic atmospheric model or by the presence of a Eurasian ice sheet. The atmospheric patterns strengthen over the next 10ky and the runaway run simulates ~30m SLE greater ice volume than the stable run (Fig. S9). The difference between the two runs at 180ka and 170ka are presented in Fig. S10. As mentioned earlier in Sect. 3.2, it is important to acknowledge the low horizontal and vertical resolutions of LOVECLIM's atmosphere, which could mean the circulation changes reported here to be model dependent.

3- Miscellaneous:
l64-78 You could refer to your figure 1 somewhere around here to facilitate the reading.

A. Done.

towards l194 and Fig. S1 From my understanding of your methods your reference climate model uses a last glacial maximum bathymetry (since bathymetry is fixed to a LGM value). Would it have been appropriate to compute the bias for the modern climate using a LGM bathymetry? More generally it would be very interesting to see the effect of the sole bathymetry on the simulated climate (under PI forcing for example).

A. Yes, LOVECLIM biases are calculated for LGM bathymetry. We agree that the impact of bathymetry on climate is interesting and important. With regard to the bias correction, we did assess the impact of using bias corrections calculated for LGM vs PI bathymetry (though not for the simulations presented in this manuscript). The figure below shows temperature and precipitation bias corrections calculated for the different bathymetries, and while there are regional differences, the large-scale structure is (surprisingly) similar. While there are other issues related to the bias correction (for example, it is not obvious that the bias should be the same under LGM and PI boundary conditions), we believe that choosing LGM vs PI bathymetry does not substantially alter the results.

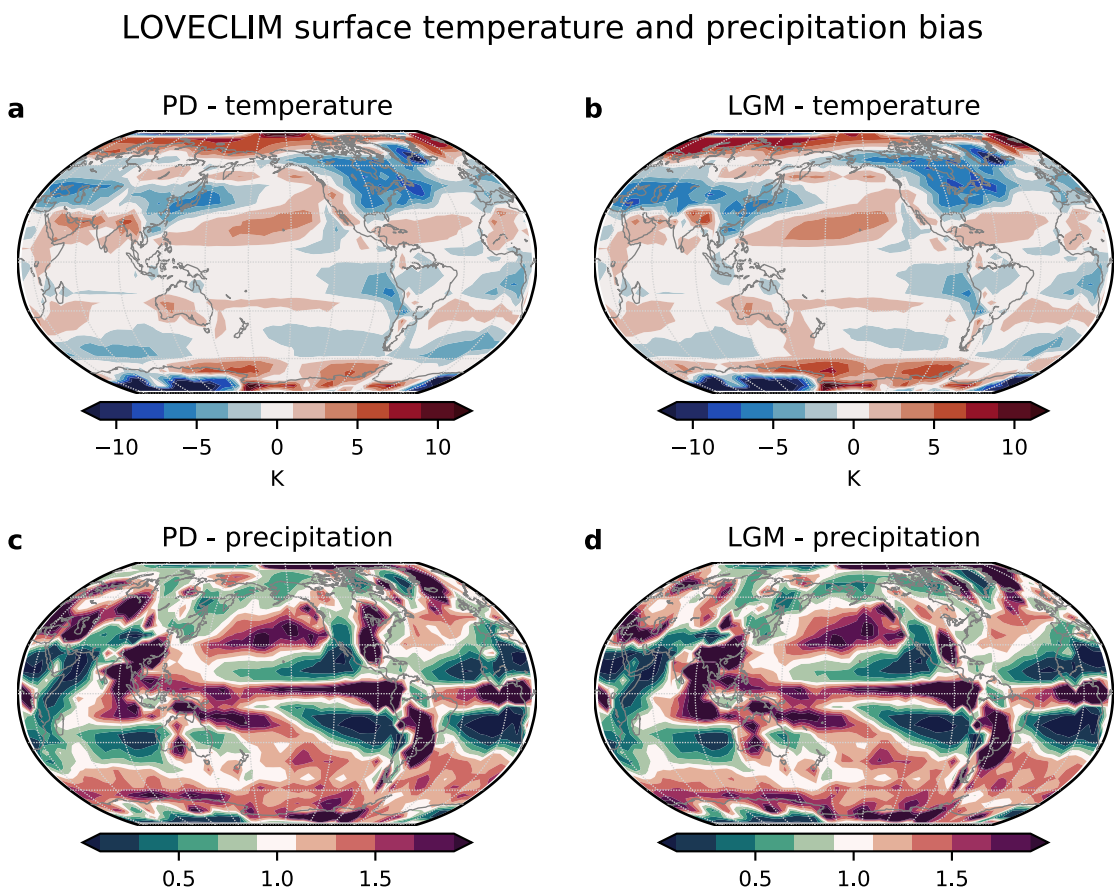

Figure R4: LOVECLIM biases for present-day simulations for temperature (a) and (b); and precipitation (c) and (d). (a) and (c) use PD bathymetry, while (b) and (d) use LGM bathymetry.

We have now clarified this in *Lines 219-233* in *Section 2.3*:

> PSUIM uses surface air temperature (T), precipitation (P), solar radiation (Q), and ocean temperature at 400m depth (T_o) as inputs from LOVECLIM. These are downscaled using a bilinear interpolation approach. The surface temperature and precipitation outputs from LOVECLIM which are used for the PSUIM surface mass balance are bias-corrected in the coupler, following Pollard and DeConto (2012), Heinemann et al. (2014) and Tigchelaar et al. (2018).
>
> $$T(t) = T_{LC}(t) + T_{obs} - T_{LC,PD} \quad (8)$$
>
> $$P(t) = P_{LC}(t) \times P_{obs}/P_{LC,PD} \quad (9)$$
>
> where T is monthly surface air temperature and P is monthly precipitation forcing from LOVECLIM at timestep t. Subscripts 'LC', 'obs' and 'LC,PD' refer to LOVECLIM chunk output, observed present day climatology, and LOVECLIM present day control run, respectively. The observed present day climatology is obtained from the European Centre for Medium-Range Weather Forecasts reanalysis dataset, ERA-40 (Uppala et al., 2005). These LOVECLIM biases are calculated for PD simulations using an LGM bathymetry. We did compare the biases between using a PD or LGM bathymetry, and while there were regional differences, the large-scale structure was found to be similar (not shown). The annual mean of the monthly mean bias correction terms $T_{obs} - T_{LC,PD}$ and $P_{obs}/P_{LC,PD}$ are presented in Fig. S1. Temperature biases in LOVECLIM for boreal summer (JJA) and austral summer (DJF) are shown in Fig. S2 for reference, since summer temperatures are more crucial for ice sheet growth and decay.

l252 The Filchner-Ronne ice shelf is advancing but there is almost no change for the Ross ice shelf. Any idea why?

A. While our simulation does not show much variations in Antarctica, the small changes over the Filchner-Ronne shelf unlike the Ross ice shelf might be because of small differences in subsurface ocean temperature. The present study focusses more on the mechanisms underlying the response of the Northern Hemisphere ice sheets, and hence we have not performed a

detailed analysis of the processes underlying the regional response of the Antarctic ice sheets and shelves. We do agree, however, that this is an interesting and important issue, that will be further explored in future studies.

l306-312 You show in the figure the mean SMB/ablation/accumulation over the ice sheet. In doing the spatial average, we can end up with very similar values for very different ice sheet extent. In addition, we cannot quantify the importance of the different processes to explain the total mass change (for example the sub-shelf melt is much more negative than SMB but it may concern only a very small fraction of the ice sheet). Instead, it could be interesting to have the integrated value over the ice sheet but not divided by the extent (Gt or km3 per year), to have a better idea of the respective role of SMB and sub-shelf melting to explain the total ice volume change.

A. We have now updated Figure 6 to show integrated values of the mass balance terms:

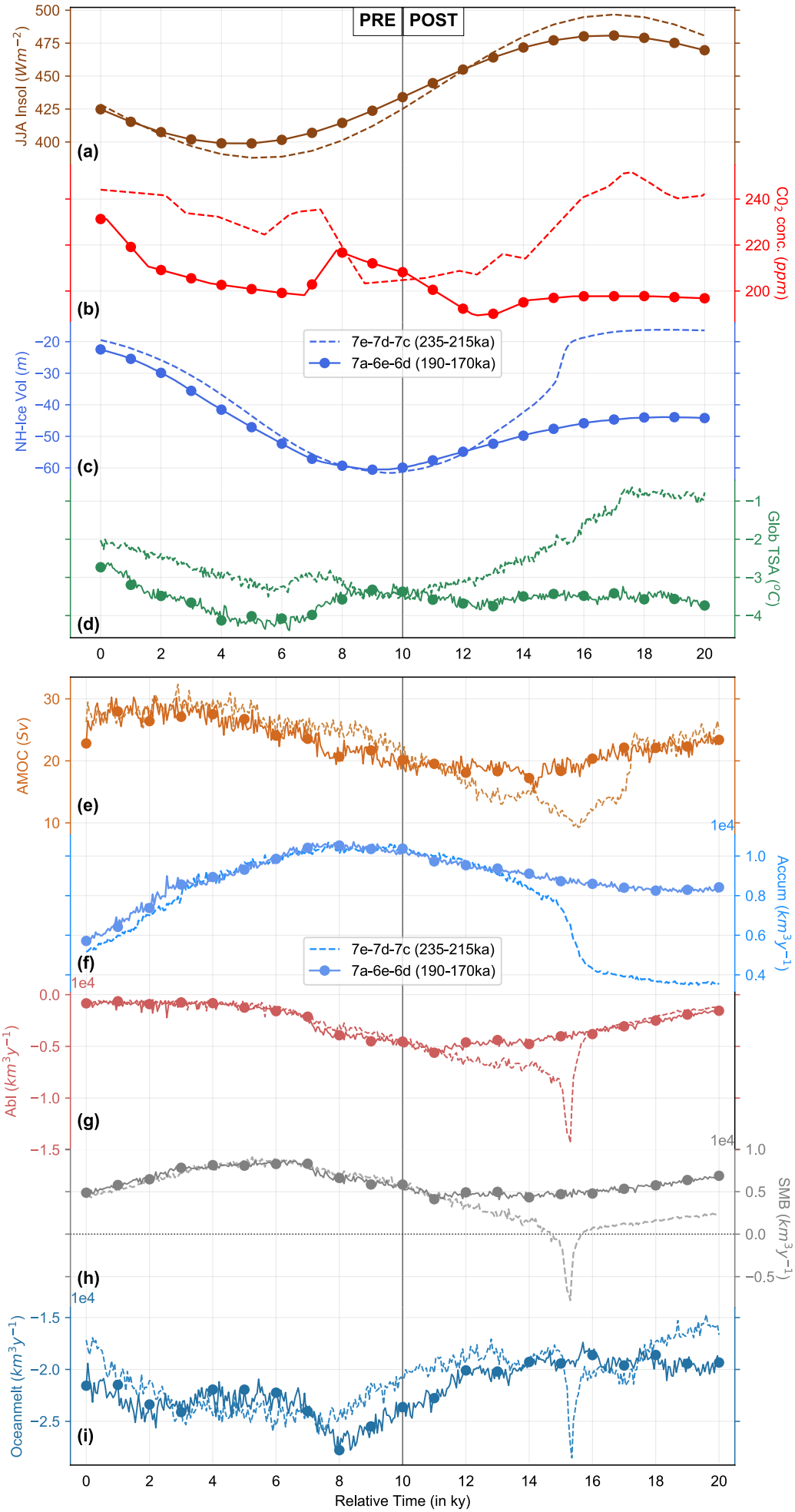
PRE
POST
JJA Insol (Wm^{-2})
(a)
CO_2 conc. (ppm)
(b)
7e-7d-7c (235-215ka)
7a-6e-6d (190-170ka)
NH-Ice Vol (m)
(c)
Glob TSA (^oC)
(d)
AMOC (Sv)
(e)
Accum (km^3y^{-1})
(f)
Abl (km^3y^{-1})
(g)
SMB (km^3y^{-1})
(h)
Oceanmelt (km^3y^{-1})
(i)
1e4
Relative Time (in ky)

Figure 6: Comparison between two glacial inception scenarios. Different variables over two 20k year periods (relative time) during pre-inception (left half) and post inception (right half) over the Northern Hemisphere are plotted. Variables from the earlier period (235-215ka) are plotted in dashed lines while that of the later period (190-170ka) are plotted in circled solid lines. (a) JJA mean insolation at 65°N (Wm^{-2}, *(Laskar et al., 2004)*). (b) CO_2 concentration (ppm, *(Lüthi et al., 2008)*). (c) Simulated Northern Hemisphere ice volume, in sea level equivalents (m). (d) Global average surface temperature anomaly (°C). (e) Temporal evolution of AMOC (Sv). (f) Net integrated accumulation rate over Northern Hemisphere ice (km^3y^{-1}). (g) Net integrated surface melt rate over Northern Hemisphere ice (km^3y^{-1}). (h) Net integrated surface mass balance over the Northern Hemisphere ice (km^3y^{-1}). (i) Net integrated subshelf melt rate over Northern Hemisphere (km^3y^{-1}).

l319-322 The spike in SMB is very impressive but I am even more surprised by the spike in shelf melting. I think it could be useful to show maps of surface mass balance and sub-shelf melting for temporal snapshots in the vicinity of this event (circa 210 ka?). In doing so, it will illustrate the saddle-collapse as well as the spike in sub- shelf melt. Again, maybe the spike in sub-shelf melt is affecting a tiny area and is not representative of the total mass loss (previous comment)?

A. The spike in subshelf melting could result from higher subsurface warming following a weakening of AMOC as reported in Liu et al. (2009) and Clark et al. (2020). We have also included a new supplementary figure, Fig. S6, showing maps of SMB and sub-shelf melting around the spikes shown in Figure 6h and 6i.

We have added the AMOC effect on subshelf melting in *Lines 418-422* in *Section 3.4*:

> For both periods the Atlantic Meridional Overturning Circulation (AMOC) is strongest during the inception phase, and weaker during termination (Fig. 6e). The AMOC weakening is substantially more pronounced in the earlier period, following the successful termination. In both periods, the AMOC recovers almost to its full interglacial state. The reduced AMOC (Fig. 6e) could lead to increased subsurface warming (Liu et al., 2009;Clark et al., 2020) causing the higher subsurface melting in Fig. 6i.

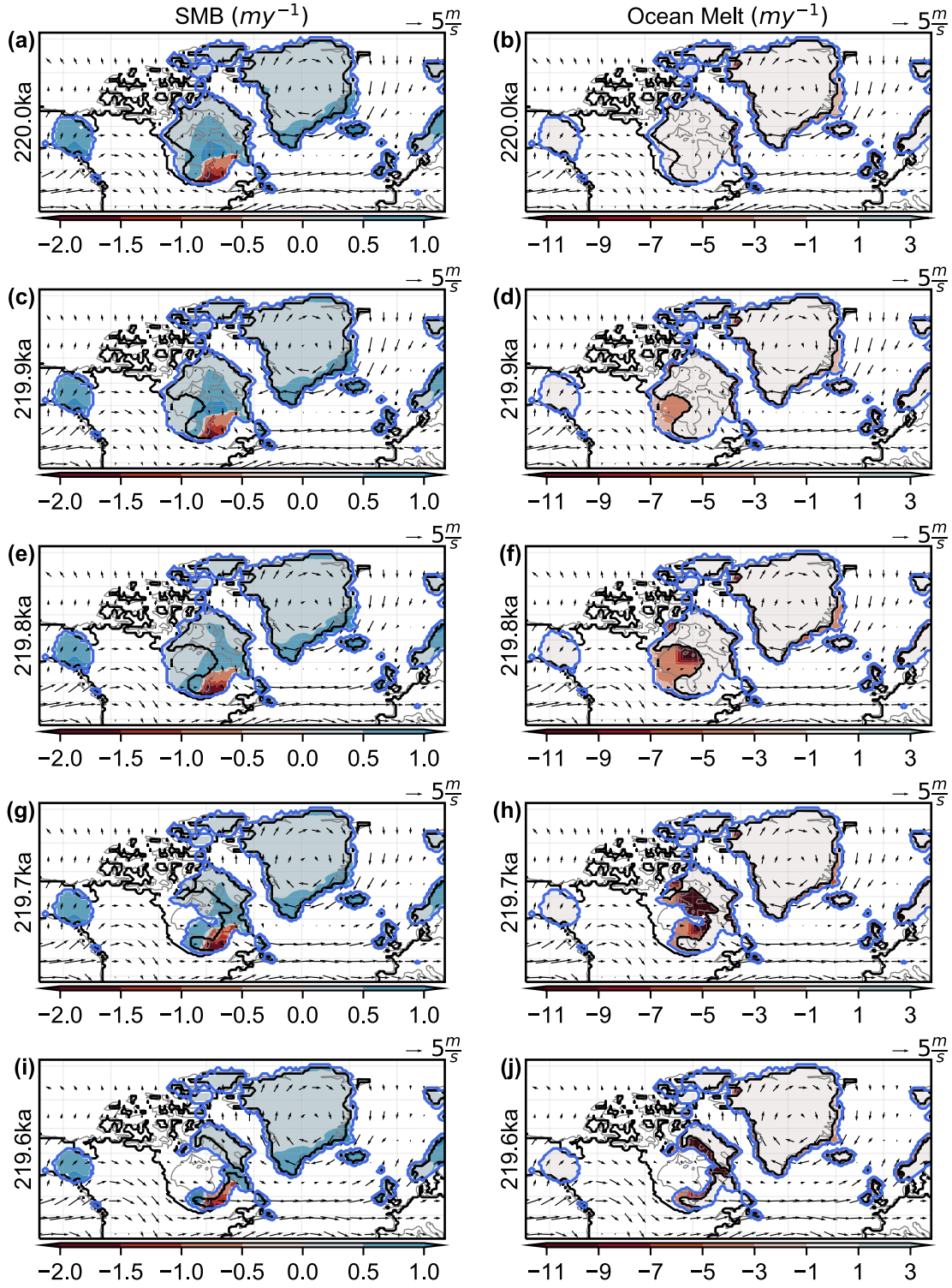

Figure S6: Temporal snapshots around the spikes in SMB and Ocean melt of Figure 6h and 6i (~15ky relative time of the dashed lines, corresponds to ~ 220ka in real time). Simulated surface mass balance (left column) and subshelf melt (right column) values at (a,b) 220ka, (c,d) 219.9ka, (e,f) 219.8ka, (g,h) 219.7ka and (I,j) 219.6ka. The blue lines mark the boundaries of the ice sheets and the black lines show the grounding line.

We have added discussions on the figure in the text in *Lines 462-469* in *Section 3.5*:

> Temporal snapshots every 0.1ky in the vicinity of the spikes in ablation (Fig. 6g), SMB (Fig. 6h) and ocean melting (Fig. 6i) are shown in Figure S6. It shows that the spikes in ablation and SMB predominantly come from a small area in the southern end of the Laurentide, while the spike in subshelf melting results only from the western part of the Laurentide with a receding grounding line. Although our model simulates sub shelf melting along the western Hudson Bay, we did not find any geologic evidence of such subsurface melting around 219.5ka. It is also worth mentioning that our setup does not simulate forebulges or other specific mechanisms modelled by more comprehensive full-Earth models. But Tigchelaar et

al. (2018) have reported such changes in mass balance arising due to changing of ice sheets to ice shelves near the grounding line.

l345-346 Do you know the reason for this? It would be nice to understand this circulation change (which produce the spike in sub-shelf melt?). It happens during the deglaciation and thus, in the meantime, you probably have a lot of freshwater flux that is discharged to the ocean. Does the two processes (increase in sub-shelf melt and freshwater flux) are related in some way? If yes, how realistic are your freshwater fluxes (see previous comment on the acceleration factor).

A. We think the spike in subsurface melt to result from relatively warm ocean waters seeping in through the gap in the grounding line on the western end of Laurentide. Following the reviewer's suggestion, Fig. S6 shows the temporal snapshots of ocean melting during the spike seen in Figure 6i. The spike in subshelf melting (Fig. 6i) as well as surface ablation (Fig. 6g) during this period would definitely lead to an increase of the freshwater flux into the ocean. This would also explain the synchronization with the AMOC slowdown seen during this period in Fig. 6e. However, since the model is run at an acceleration and we are conserving the freshwater flux, the net freshwater volume dumped into the ocean would be underestimated and thus freshwater flux changes from PSUIM into LOVECLIM may not be very realistic.

We have now discussed this in *Lines 461-473* in *Section 3.5*:

Further, relatively warm subsurface ocean water (>-1˚C) seeps along the west bank of Hudson Bay leading to a more pronounced negative mass balance (Fig. S5d). This shows up as a spike in the subsurface ocean melt values in Fig. 6i. Temporal snapshots every 0.1ky in the vicinity of the spikes in ablation (Fig. 6g), SMB (Fig. 6h) and ocean melting (Fig. 6i) are shown in Figure S6. It shows that the spikes in ablation and SMB predominantly come from a small area in the southern end of the Laurentide, while the spike in subshelf melting results only from the western part of the Laurentide with a receding grounding line. Although our model simulates sub shelf melting along the western Hudson Bay, we did not find any geologic evidence of such subsurface melting around 219.5ka. It is also worth mentioning that our setup does not simulate forebulges or other specific mechanisms modelled by more comprehensive full-Earth models. But Tigchelaar et al. (2018) have reported such changes in mass balance arising due to changing of ice sheets to ice shelves near the grounding line. The spike in subshelf melting (Fig. 6i) as well as surface ablation (Fig. 6g) during this period lead to an increase of the freshwater flux into the ocean. This could explain the synchronization with the AMOC slowdown seen during this period in Fig. 6e. However, since our model is run at an acceleration ($N_A = 5$) and we conserve the freshwater flux (Sec. 2.3), the total freshwater volume dumped into the ocean is being underestimated, which may distort the LOVECLIM response.

Fig. 2 You could also mention on the figure how the interpolation / downscaling to the different grids is done. Also, by "landmask" you mean "ice mask" (albedo)?

A. We have clarified that we use first order conservative remapping to interpolate the data across the different grids. These are mentioned in *Line 219-220* in *Section 2.3*:

PSUIM uses surface air temperature (T), precipitation (P), solar radiation (Q), and ocean temperature at 400m depth (T_o) as inputs from LOVECLIM. These are downscaled using a bilinear interpolation approach.

"Land mask" means "ice mask" in Figure 2. We have now changed this.

Technical comments:

Fig. 4 The grounding line is hardly distinguishable.

A. We have now changed it to solid green lines for all the figures.

Fig. 4 (and Fig. S2, S3, S4 and S5) I find the maps of mixed information thickness / ice velocity hard to read. Maybe using the contours for thickness and the solid colours for velocity would look nicer?

A. Done. We have also applied the same to Figure 7, S3, S6, S6 and S8. The updated Fig. 7 is attached here as an example.

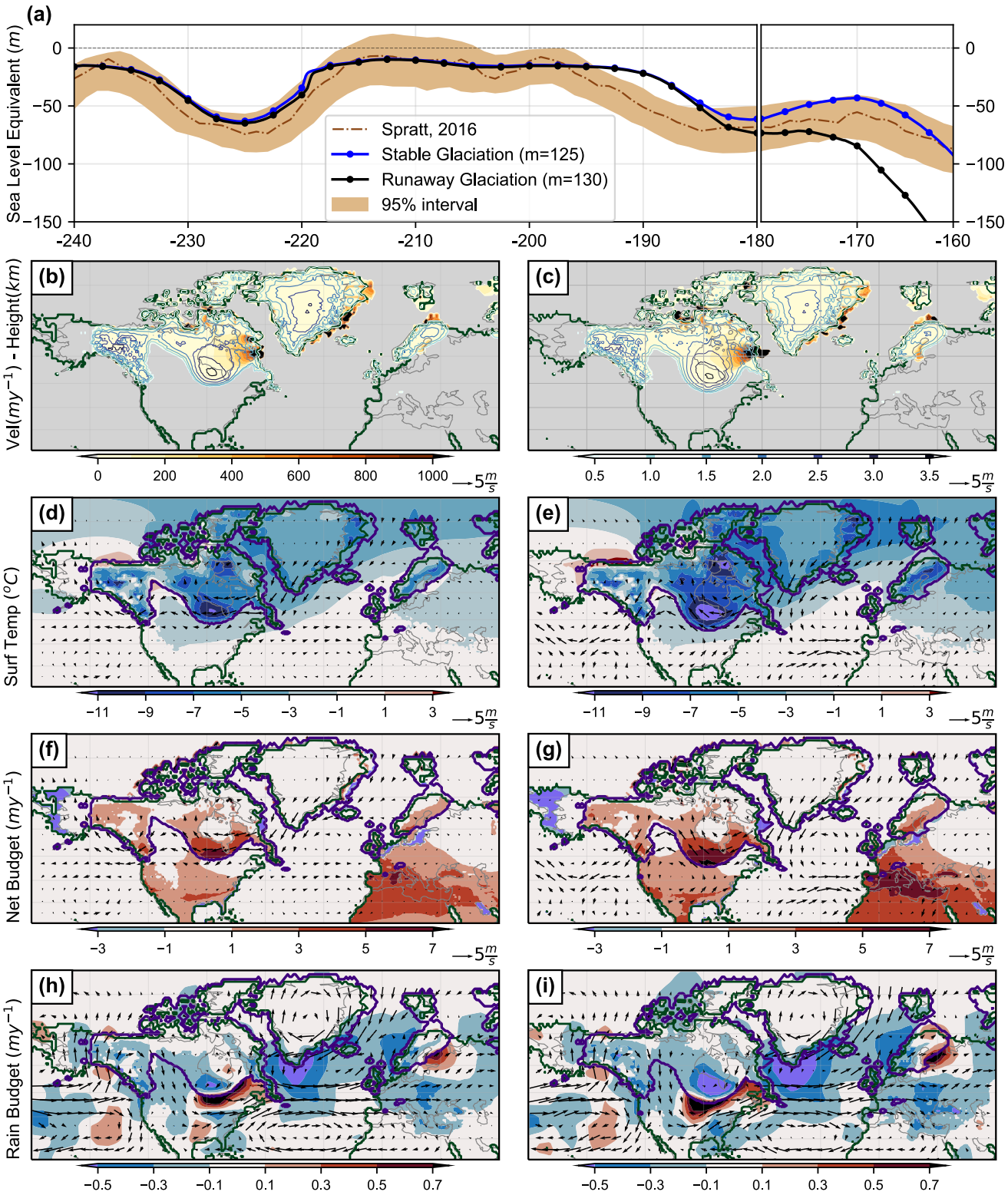

Figure 7: Bifurcation of the system at 180ka while transitioning into MIS 6 over Laurentide. (a) Sea level reconstruction (m) and 95% confidence interval of Spratt and Lisiecki (2016) (brown). Total ice volume (in terms of SLE, m) from two ensemble members of LOVECLIP, one that leads to a stable glacial inception (blue; α=2, m=125 Wm^{-2}) and another into a runaway glaciation (black; α=2, m=130 Wm^{-2}). Climate and ice sheet variables at 180ka from the stable glaciation on the left column (b, d, f and h) and runaway glaciation on the right (c, e, g and i). (b,c) Basal ice velocity (solid colors, my^{-1}) overlaid with ice thickness (colored contours, km) and the grounding line (solid green lines). (d,e) Surface temperature anomalies ($^\circ C$) overlaid with *anomalous* wind vectors at 800hPa (ms^{-1}). (f,g) Net mass balance anomalies (my^{-1}) overlaid with *anomalous* winds (ms^{-1}). (h,i) Rainfall anomalies (my^{-1}) overlaid with *absolute* winds (ms^{-1}). The purple contours in (d) to (i) mark the boundaries of the ice sheets from each run (stable for left and runaway for right). Anomalies here are with respect to the initial condition at 240ka. Anomalies over the Eurasian and Siberian ice sheets are small and not shown.

Fig. 7 I am sure that you can use a better colourbar for panel f to i. At least it can be white where there are small changes instead of yellow.

A. We now use a better color scheme for Figure 7, S8 and S9. For instance, see figure above.

Fig. 7 l675 purple contours are for which run (blue or black in panel a)?

A. The purple contours mark the boundaries of the ice sheets simulated in each experiment, the left one is from the blue line and the right one from the black line. We have now clarified this in the figure caption (see above).

Fig. S1 Panel b: since a multiplicative correction of 1 means no correction maybe it could have been better to have a neutral colour such as white around the value of 1.

A. Done.

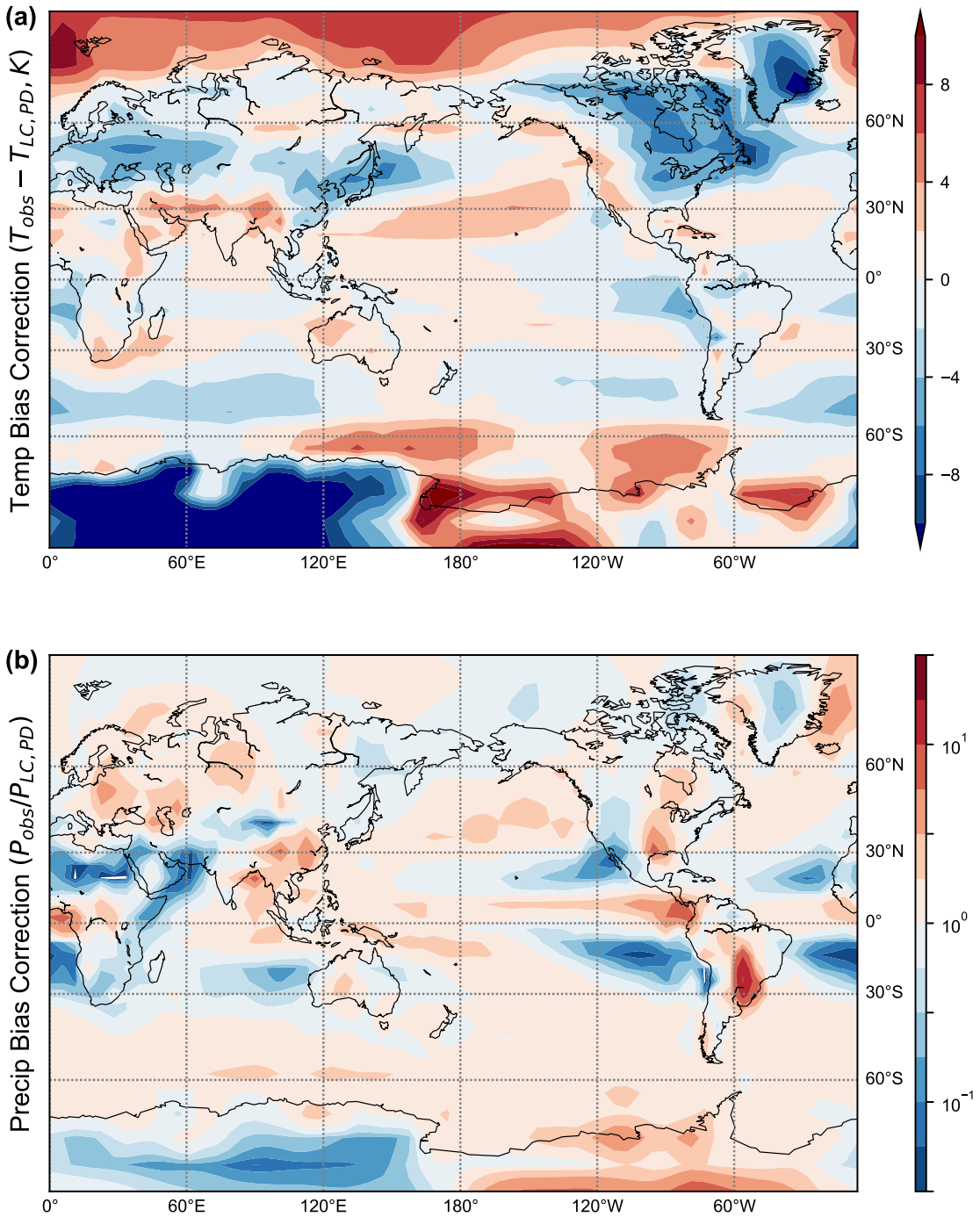

Figure S1: Bias correction used for LOVECLIM outputs. (a) Additive bias correction for annual mean surface temperature (K). (b) Multiplicative bias correction for annual mean precipitation. Colours are log normalised for the precipitation case.

Reference:

Bahadory, T., and Tarasov, L.: LCice 1.0 – a generalized Ice Sheet System Model coupler for LOVECLIM version 1.3: description, sensitivities, and validation with the Glacial Systems Model (GSM version D2017.aug17), Geoscientific Model Development, 11, 3883-3902, 10.5194/gmd-11-3883-2018, 2018.

Batchelor, C. L., Margold, M., Krapp, M., Murton, D. K., Dalton, A. S., Gibbard, P. L., Stokes, C. R., Murton, J. B., and Manica, A.: The configuration of Northern Hemisphere ice sheets through the Quaternary, Nature communications, 10, 1-10, 2019.

Clark, P. U., He, F., Golledge, N. R., Mitrovica, J. X., Dutton, A., Hoffman, J. S., and Dendy, S.: Oceanic forcing of penultimate deglacial and last interglacial sea-level rise, Nature, 577, 660-664, 2020.

Colleoni, F., Masina, S., Cherchi, A., Navarra, A., Ritz, C., Peyaud, V., and Otto-Bliesner, B.: Modeling Northern Hemisphere ice-sheet distribution during MIS 5 and MIS 7 glacial inceptions, Climate of the Past, 10, 269-291, 10.5194/cp-10-269-2014, 2014.

Colleoni, F., and Liakka, J.: Transient simulations of the Eurasian ice sheet during the Saalian glacial cycle, SVENSK KÄRNBRÄNSLEHANTERING AB, StockholmSKB TR-19-17, 2020.

Edwards, T. L., Brandon, M. A., Durand, G., Edwards, N. R., Golledge, N. R., Holden, P. B., Nias, I. J., Payne, A. J., Ritz, C., and Wernecke, A.: Revisiting Antarctic ice loss due to marine ice-cliff instability, Nature, 566, 58-64, 10.1038/s41586-019-0901-4, 2019.

Friedrich, T., and Timmermann, A.: Using Late Pleistocene sea surface temperature reconstructions to constrain future greenhouse warming, Earth and Planetary Science Letters, 530, 115911, 2020.

Heinemann, M., Timmermann, A., Elison Timm, O., Saito, F., and Abe-Ouchi, A.: Deglacial ice sheet meltdown: orbital pacemaking and CO 2 effects, Climate of the Past, 10, 2014.

Jongma, J. I., Driesschaert, E., Fichefet, T., Goosse, H., and Renssen, H.: The effect of dynamic–thermodynamic icebergs on the Southern Ocean climate in a three-dimensional model, Ocean Modelling, 26, 104-113, 2009.

Laskar, J., Robutel, P., Joutel, F., Gastineau, M., Correia, A., and Levrard, B.: A long-term numerical solution for the insolation quantities of the Earth, Astronomy & Astrophysics, 428, 261-285, 2004.

Le Morzadec, K., Tarasov, L., Morlighem, M., and Seroussi, H.: A new sub-grid surface mass balance and flux model for continental-scale ice sheet modelling: testing and last glacial cycle, Geoscientific Model Development, 8, 3199, 2015.

Liu, Z., Otto-Bliesner, B., He, F., Brady, E., Tomas, R., Clark, P., Carlson, A., Lynch-Stieglitz, J., Curry, W., and Brook, E.: Transient simulation of last deglaciation with a new mechanism for Bølling-Allerød warming, Science, 325, 310-314, 2009.

Locarnini, R. A., Mishonov, A. V., Antonov, J. I., Boyer, T. P., Garcia, H. E., Baranova, O. K., Zweng, M. M., Paver, C. R., Reagan, J. R., and Johnson, D. R.: World ocean atlas 2013. Volume 1, Temperature, 2013.

Lofverstrom, M., and Liakka, J.: The influence of atmospheric grid resolution in a climate model-forced ice sheet simulation, Cryosphere, 12, 2018.

Lüthi, D., Le Floch, M., Bereiter, B., Blunier, T., Barnola, J.-M., Siegenthaler, U., Raynaud, D., Jouzel, J., Fischer, H., Kawamura, K., and others: High-resolution carbon dioxide concentration record 650,000--800,000 years before present, Nature, 453, 379-379, 2008.

Pollard, D., and DeConto, R. M.: Description of a hybrid ice sheet-shelf model, and application to Antarctica, Geoscientific Model Development, 5, 1273-1295, 10.5194/gmd-5-1273-2012, 2012.

Pollard, D., DeConto, R. M., and Alley, R. B.: Potential Antarctic Ice Sheet retreat driven by hydrofracturing and ice cliff failure, Earth and Planetary Science Letters, 412, 112-121, 10.1016/j.epsl.2014.12.035, 2015.

Roche, D. M., Dumas, C., Bügelmayer, M., Charbit, S., and Ritz, C.: Adding a dynamical cryosphere to iLOVECLIM (version 1.0): coupling with the GRISLI ice-sheet model, Geoscientific Model Development, 7, 1377-1394, 10.5194/gmd-7-1377-2014, 2014.

Roe, G. H., and Lindzen, R. S.: The mutual interaction between continental-scale ice sheets and atmospheric stationary waves, Journal of Climate, 14, 1450-1465, 2001.

Rohling, E. J., Hibbert, F. D., Williams, F. H., Grant, K. M., Marino, G., Foster, G. L., Hennekam, R., De Lange, G. J., Roberts, A. P., and Yu, J.: Differences between the last two glacial maxima and implications for ice-sheet, δ18O, and sea-level reconstructions, Quaternary Science Reviews, 176, 1-28, 2017.

Schloesser, F., Friedrich, T., Timmermann, A., DeConto, R. M., and Pollard, D.: Antarctic iceberg impacts on future Southern Hemisphere climate, Nature Climate Change, 9, 672-677, 2019.
Spratt, R. M., and Lisiecki, L. E.: A Late Pleistocene sea level stack, Climate of the Past, 12, 1079-1092, 2016.
Svendsen, J. I., Alexanderson, H., Astakhov, V. I., Demidov, I., Dowdeswell, J. A., Funder, S., Gataullin, V., Henriksen, M., Hjort, C., and Houmark-Nielsen, M.: Late Quaternary ice sheet history of northern Eurasia, Quaternary Science Reviews, 23, 1229-1271, 2004.
Tigchelaar, M., Timmermann, A., Pollard, D., Friedrich, T., and Heinemann, M.: Local insolation changes enhance Antarctic interglacials: Insights from an 800,000-year ice sheet simulation with transient climate forcing, Earth and Planetary Science Letters, 495, 69-78, 10.1016/j.epsl.2018.05.004, 2018.
Timm, O., and Timmermann, A.: Simulation of the last 21 000 years using accelerated transient boundary conditions, Journal of Climate, 20, 4377-4401, 2007.
Timm, O., Köhler, P., Timmermann, A., and Menviel, L.: Mechanisms for the onset of the African Humid Period and Sahara Greening 14.5–11 ka BP, Journal of Climate, 23, 2612-2633, 2010.
Timmermann, A., and Friedrich, T.: Late Pleistocene climate drivers of early human migration, Nature, 538, 92-95, 10.1038/nature19365, 2016.
Ullman, D., LeGrande, A., Carlson, A. E., Anslow, F., and Licciardi, J.: Assessing the impact of Laurentide Ice-Sheet topography on glacial climate, 2014.
Uppala, S. M., Kållberg, P., Simmons, A., Andrae, U., Bechtold, V. D. C., Fiorino, M., Gibson, J., Haseler, J., Hernandez, A., and Kelly, G.: The ERA-40 re-analysis, Quarterly Journal of the Royal Meteorological Society: A journal of the atmospheric sciences, applied meteorology and physical oceanography, 131, 2961-3012, 2005.
Zhang, Z., Yan, Q., Zhang, R., Colleoni, F., Ramstein, G., Dai, G., Jakobsson, M., O'Regan, M., Liess, S., Rousseau, D. D., Wu, N., Farmer, E. J., Contoux, C., Guo, C., Tan, N., and Guo, Z.: Rapid waxing and waning of Beringian ice sheet reconcile glacial climate records from around North Pacific, Clim. Past Discuss., 2020, 1-25, 10.5194/cp-2020-38, 2020.